https://doi.org/10.5194/egusphere-2026-3198
Preprint. Discussion started: 21 August 2026

Potential use of radar slant-linear depolarization for measuring rainfall microphysics

Hao Huang[1,2,3], Chen Lu[1,2], Wenxuan Zhao[1,2], Kun Zhao[1,2,3], and Xing Wang[4,2]

1 State Key Laboratory of Severe Weather Meteorological Science and Technology, Nanjing University, Nanjing, China

2 Key Laboratory of Mesoscale Severe Weather of MOE, and School of Atmospheric Sciences, Nanjing University, Nanjing, China

3 Key Laboratory of Radar Meteorology, China Meteorology Administration, Beijing, China

4 School of Computer Engineering, Nanjing Institute of Technology, Nanjing, China

Correspondence: Hao Huang (huanghao@nju.edu.cn)

Abstract. Single-transmit, dual-receive millimeter-wave radars can be attractive for compact and scanning precipitation observations, but they do not necessarily provide the conventional horizontal/vertical dual-polarization variables used to constrain raindrop size distributions. This study evaluates whether a fixed slant-linear basis can turn the weak backscattering anisotropy of oblate raindrops into a useful liquid-rain observable. In the proposed geometry, a +45° transmitted polarization and co-/cross-slant receive channels project the difference between horizontal and vertical co-polar backscattering amplitudes into an orthogonal-slant return. We use explicit T-matrix scattering calculations, normalized-gamma and observed drop size distributions, and controlled neural-regression diagnostics to quantify the information content and observability of the resulting slant-linear depolarization ratio (SLDR). For the baseline Ka-band gamma ensemble, the reflectivity (Z_+)–SLDR space separates characteristic drop size and concentration that are ambiguous under reflectivity alone. With 1 dB SLDR uncertainty, adding SLDR reduces the independent-test RMSE of mass-weighted mean diameter (D_m) from 0.672 to 0.243 mm and reduces the RMSE of log-transformed rain rate ($\log_{10}R$) from 0.163 to 0.055. The same sign of improvement persists for Nanjing 2DVD, EPFL HyMeX, NASA IFLOODS, and variable-shape gamma checks. Sensitivity tests show that random SLDR uncertainty degrades retrievals gradually, whereas relative co-/cross-slant gain bias and polarization leakage define stronger practical constraints. Through the controlled forward-simulation information-content tests, SLDR is identified as a physically distinct measurement coordinate for liquid-rain microphysics. The calibration and detectability conditions are also defined for a field test with suitable single-transmit, dual-receive radars.

1 Introduction

Millimeter-wave and cloud-radar systems are increasingly used for high-resolution observations of clouds and precipitation, including compact, mobile, vertically pointing, and scanning deployments (Kollias et al., 2007). Many Ka- and W-band cloud-radar implementations are attractive for such applications because they can provide sensitive Doppler measurements with relatively compact hardware. A common polarimetric configuration in these systems is to transmit a single linear polarization and receive co- and cross-polarized components, as in LDR-mode Ka-band cloud radars such as MIRA-35 (Görsdorf et al., 2015; Teisseire et al., 2024). This architecture is attractive from an engineering perspective, but it does not automatically provide the conventional horizontal/vertical (H/V) dual-polarization variables used by weather radars. In particular, reflectivity alone

https://doi.org/10.5194/egusphere-2026-3198
Preprint. Discussion started: 21 August 2026

cannot determine whether a rain echo is produced by many small drops or by fewer larger drops. Conventional dual-polarization weather radars reduce this ambiguity using differential reflectivity and related H/V observables (Bringi & Chandrasekar, 2001; Bringi et al., 2003; Seliga & Bringi, 1976; Zhang, 2016), but these measurements may not be available in simpler single-transmit, dual-receive architectures.

An orthogonal receive channel can provide useful information only if the observing geometry projects a physically meaningful scattering contrast into that channel. For statistically horizontally oriented liquid raindrops, the conventional H/V backscattering matrix is nearly diagonal, so ordinary H/V cross-polar power is usually a weak rain-microphysics observable (Bringi & Chandrasekar, 2001; Sandford et al., 2017). The missing element is therefore not merely a second receiver, but a transmit/receive basis that converts the H/V co-polar scattering contrast of oblate drops into a measurable component.

A fixed 45° slant-linear basis provides such a geometry. A +45° transmitted field samples the H and V scattering axes equally; if an oblate raindrop scatters the two components differently, the scattered field is no longer aligned with the transmitted slant state and has power in the orthogonal slant receive channel. The resulting slant-linear depolarization ratio (SLDR) is not a transformation of reflectivity. It is a separate polarization power ratio controlled by the raindrop shape-dependent contrast between H and V co-polar backscattering amplitudes.

SLDR-mode measurements have mainly been used for hydrometeor-shape sensing in cloud and ice studies, where nonsphericity can produce strong depolarization signals. For example, slant-linear depolarization has been used with scanning W-band radar observations to infer ice crystal habits (Matrosov et al., 2012), and more recently with a 35 GHz scanning cloud radar to determine the vertical distribution of in-cloud particle shape (Teisseire et al., 2024). Its value for liquid rain is less established. Raindrops are only weakly to moderately nonspherical, the millimeter-wave scattering response can become non-Rayleigh for larger drops, and the cross-slant return may approach receiver-noise or polarization-leakage floors (Matrosov, 2021). These issues make rainfall SLDR a measurement-design problem as well as a scattering-information problem.

For liquid rain, SLDR is useful only if two conditions are met. From a microphysical perspective, it must provide a constraint that is not already contained in reflectivity, such as sensitivity to characteristic drop size at a given echo strength. From an observational perspective, the hydrometeor-generated cross-slant power must remain distinguishable from receiver noise, polarization leakage, and relative channel-calibration errors. These considerations motivate a combined assessment of SLDR information content and first-order observability constraints.

This paper evaluates the information content and observability of SLDR for liquid-rain microphysics. We use explicit fixed-basis T-matrix scattering calculations to (1) derive the slant-basis measurement coordinate, (2) test how the joint co-slant reflectivity–SLDR space organizes drop size distribution (DSD) variability, (3) quantify the information added by SLDR using controlled neural-regression diagnostics, (4) test consistency with measured DSD spectra and a variable-shape gamma prior, and (5) translate the information-content result into constraints on random SLDR uncertainty, relative co-/cross-slant gain bias, polarization isolation, and cross-slant detectability. Ka band is used as the main demonstration frequency because it is relevant to compact and cloud-radar systems and because millimeter-size raindrops produce appreciable H/V scattering contrast, but the basis-rotation mechanism itself is not specific to one wavelength.

The paper is organized as follows. Section 2 describes the slant-basis measurement geometry, scattering calculations, DSD data sets, neural-regression diagnostics, and observability tests. Section 3 presents the simulated information content, retrieval diagnostics, consistency checks, and field-implementation constraints.

https://doi.org/10.5194/egusphere-2026-3198
Preprint. Discussion started: 21 August 2026

Section 4 discusses the physical interpretation, practical implications, and limitations of the proposed rainfall SLDR measurement. The paper ends with conclusions in Sect. 5.

2 Methods

2.1 Slant-basis measurement geometry

For a monostatic backscatter measurement with one transmitted polarization and two calibrated orthogonal receive channels, the nearly diagonal H/V scattering matrix of statistically horizontally oriented liquid raindrops can be sampled in a rotated polarization basis. In the ideal diagonal limit,

$$\mathbf{S}_{HV} \approx \begin{pmatrix} S_{HH} & 0 \\ 0 & S_{VV} \end{pmatrix} \tag{1}$$

where S_{HH} and S_{VV} are the H- and V-polarized co-polar backscattering amplitudes expressed in a common incident/received H/V basis. In the numerical implementation, the monostatic backscatter receive-basis convention is converted to this common H/V basis before the slant projection, so an isotropic particle has $S_{HH} = S_{VV}$ and produces no orthogonal-slant power.

A +45° slant transmit state and its orthogonal receive state are

$$\mathbf{s}_{+} = \frac{\mathbf{H} + \mathbf{V}}{\sqrt{2}} \tag{2a}$$

$$\mathbf{s}_{-} = \frac{\mathbf{H} - \mathbf{V}}{\sqrt{2}} \tag{2b}$$

Projection of the scattered field onto the co-slant and orthogonal-slant receive states gives

$$E_{+} \propto \mathbf{s}_{+}^{T} \mathbf{S}_{HV} \mathbf{s}_{+} = \frac{S_{HH} + S_{VV}}{2} \tag{3a}$$

$$E_{-} \propto \mathbf{s}_{-}^{T} \mathbf{S}_{HV} \mathbf{s}_{+} = \frac{S_{HH} - S_{VV}}{2} \tag{3b}$$

Thus, the orthogonal-slant channel is proportional to the H/V co-polar amplitude difference, not to ordinary H/V cross-polar scattering. The 45° angle is a radar polarization-basis angle; it does not imply that the raindrops are physically canted by 45°. This basis-rotation mechanism is illustrated in Fig. 1.

The same result can be written as a basis rotation. Defining

$$\mathbf{R} = [\mathbf{s}_{+}\ \mathbf{s}_{-}] = \frac{1}{\sqrt{2}} \begin{pmatrix} 1 & 1 \\ 1 & -1 \end{pmatrix} \tag{4}$$

the scattering matrix expressed in the slant basis is

$$\mathbf{S}_{\mathrm{slant}} = \mathbf{R}^{T} \mathbf{S}_{HV} \mathbf{R} \tag{5}$$

For the ideal diagonal H/V matrix this gives

$$\mathbf{S}_{\mathrm{slant}} = \frac{1}{2} \begin{pmatrix} S_{HH} + S_{VV} & S_{HH} - S_{VV} \\ S_{HH} - S_{VV} & S_{HH} + S_{VV} \end{pmatrix} \tag{6}$$

The off-diagonal element in the slant basis is therefore generated by the H/V co-polar contrast of the particle. Alternative monostatic receive-basis sign conventions can change the signs of individual complex amplitudes, but they do not change the co- and cross-slant powers or the resulting SLDR.

For a DSD, randomly distributed drops contribute incoherently, so the bulk co- and cross-slant powers are obtained by integrating single-particle powers rather than complex amplitudes:

$$P_{+} \propto \int N(D) \int p(\psi) |E_{+}(D,\psi)|^2 \, d\psi \, dD \tag{7a}$$

$$P_{-} \propto \int N(D) \int p(\psi) |E_{-}(D,\psi)|^2 \, d\psi \, dD \tag{7b}$$

https://doi.org/10.5194/egusphere-2026-3198
Preprint. Discussion started: 21 August 2026

where D is equivolume diameter, $N(D)$ is the DSD, ψ is the physical canting angle relative to the horizontally aligned equilibrium orientation, and $p(\psi)$ is the canting-angle distribution. SLDR is then defined from noise-corrected powers as

$$\mathrm{SLDR} = 10\log_{10}\left(\frac{P_-}{P_+}\right) \tag{8}$$

For a single particle in the ideal diagonal limit, the common factor of 1/2 in E_+ and E_- cancels in the power ratio, giving the diagnostic interpretation

$$\mathrm{SLDR_{sp}} = 10\log_{10}\left(\frac{|S_{HH} - S_{VV}|^2}{|S_{HH} + S_{VV}|^2}\right) \tag{9}$$

This expression explains why SLDR directly senses raindrop-shape contrast, while the DSD-integrated definition above is used for bulk radar variables because randomly positioned drops add in power rather than coherent amplitude.

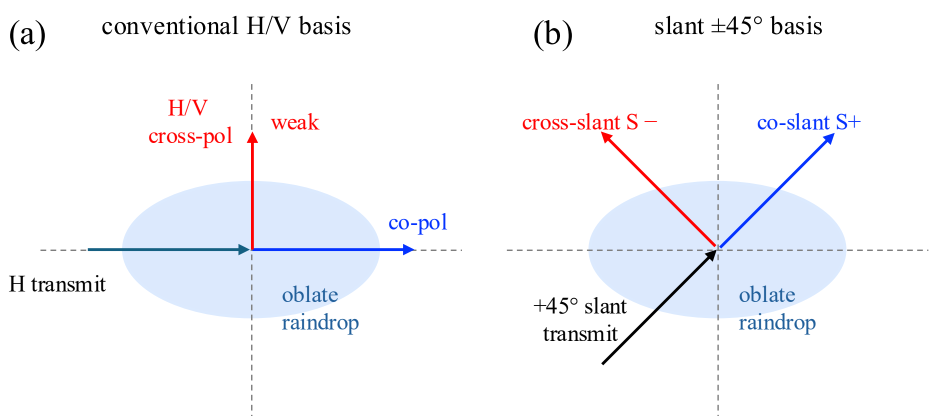

Figure 1. Basis-rotation concept of slant-linear depolarization in liquid rain (illustrated by an oblate raindrop). (a) In the conventional H/V basis, a horizontally oriented oblate raindrop produces a strong co-polar return but little cross-polar return in the ideal diagonal-scattering limit. (b) In a slant $\pm 45^\circ$ basis, the transmitted field samples both H and V scattering axes, so the H/V backscattering contrast appears as an orthogonal slant return. The 45° angle denotes the radar transmit/receive polarization basis and not a 45° raindrop canting angle.

2.2 Scattering model and DSD data sets

The scattering calculations use a T-matrix model for oblate liquid raindrops (Leinonen, 2014). The baseline frequency is 35 GHz, representative of Ka-band cloud-radar implementations. Liquid-water permittivity is evaluated at 20 °C (Liebe et al., 1991), and raindrops are represented as oblate spheroids with empirical size-dependent axis ratios from Brandes et al. (2002) and Thurai and Bringi (2005). The baseline orientation is horizontally aligned; canting sensitivity is evaluated separately with zero-mean physical canting distributions with standard deviations of 5° and 10°. For each particle size and orientation, the H/V backscattering matrix is projected explicitly onto the fixed +45°/ −45° radar basis before power averaging and DSD integration.

The main synthetic experiment draws 20000 normalized gamma DSDs (Ulbrich, 1983), with D_m sampled uniformly over 0.5–4.0 mm, $\log_{10}N_w$ sampled uniformly over 2–5, and fixed shape parameter $\mu = 3$. Samples are retained only when the forward-modeled variables are finite, $0 < Z_+ < 65$ dBZ, $D_m > 0.3$ mm, precipitation variables are positive, and $R \leq 200$ mm h^{-1}. The rain-rate upper bound is an evaluation-domain

https://doi.org/10.5194/egusphere-2026-3198
Preprint. Discussion started: 21 August 2026

choice that avoids raw-error metrics being dominated by a small number of extremely high-rain-rate states for which Ka-band attenuation would be a dominant unmodeled uncertainty. The fixed-μ baseline contains 15283 valid samples.

To test whether the result depends on the uniform gamma prior, we repeat the forward modeling with measured DSD spectra. The Nanjing 2DVD data, collected during the summers of 2014–2017, contain 60856 valid spectra after applying the same filtering criteria (Wen et al., 2019). Two public Parsivel subsets are also used: EPFL HyMeX LTE SOP3 station 20 in France (Berne et al., 2023) and NASA IFLOODS apu01 in Iowa, USA (NASA, 2025). Raw Parsivel drop-count spectra are converted to $N(D)$ using published diameter and velocity bins, a drop-size-dependent effective sampling area, and the native sampling intervals. Spectra with fewer than 50 drops are removed, sparse tail bins above 8.3 mm are excluded to match the scattering grid, and the same evaluation-domain filters are applied after scattering. The filtered totals are 5907 spectra for EPFL HyMeX and 5945 spectra for NASA IFLOODS.

2.3 Neural-regression information-content diagnostic

To evaluate the additional information carried by SLDR, we frame the problem as a controlled supervised-regression experiment. The goal is not to develop an operational rainfall retrieval algorithm, but to compare how well the same regression framework can infer rain microphysical quantities from reflectivity alone and from reflectivity combined with SLDR. Two multilayer perceptron (MLP) configurations are therefore trained and tested using the same data splits and training procedure. The first uses Z_+ in dBZ as a one-dimensional input, whereas the second uses the two-dimensional input vector $(Z_+,$ SLDR), with SLDR expressed in dB. The primary retrieval targets are D_m and $\log_{10}R$ (with the other variables verified). For rain rate, RMSE, and median absolute relative error (MedARE) are also computed in linear (R) space after back-transforming the $\log_{10}R$ predictions.

All data sets are split into 80% training and 20% independent testing samples, with 15% of the training subset reserved for validation. Input features and targets are standardized using the training subset and inverse-transformed after prediction. The MLP has two hidden layers with 128 and 64 units, rectified linear activations, batch normalization, and 0.05 dropout. It is optimized with AdamW using a learning rate of 10^{-3}, weight decay of 10^{-4}, batch size of 512, and Smooth L1 loss with $\beta = 0.5$. Training is allowed for up to 350 epochs, with early stopping after 35 epochs without validation-loss improvement and gradient clipping at a norm of 5.0.

Three feature/error configurations are evaluated: a Z-only baseline, a clean Z–SLDR case using unperturbed SLDR, and a noisy Z–SLDR case with 1 dB Gaussian perturbations applied to SLDR. The 1 dB perturbation is an information-content sensitivity scale comparable to the approximately 1.3 dB internal calibration accuracy reported for a long-term 35 GHz MIRA-35 cloud radar system (Görsdorf et al., 2015), although real SLDR uncertainty also depends on cross-slant noise, leakage, and channel calibration. The noisy two-input MLP is trained with matching SLDR-noise augmentation: the clean training set is retained, and two additional noisy SLDR copies are added for each training sample.

2.4 Measurement-error and observability tests

To connect the information-content analysis with field implementation, we consider two types of practical limitations. First, we define measurement and microphysical perturbations that are applied to the forward-modeled SLDR retrieval framework and evaluated in Sect. 3.4. Second, we derive first-order signal-to-noise and leakage-floor relations that indicate when the hydrometeor-generated cross-slant return can be interpreted as a measurable radar signal. These relations are not intended to represent a complete radar-system simulator; rather, they provide simple observability constraints for interpreting the retrieval diagnostics.

https://doi.org/10.5194/egusphere-2026-3198
Preprint. Discussion started: 21 August 2026

Random SLDR uncertainty is represented as a zero-mean Gaussian perturbation added to the forward-modeled SLDR. Systematic relative co-/cross-slant gain bias is represented as an additive SLDR offset,

$$\mathrm{SLDR_{meas}} = \mathrm{SLDR_{true}} + \Delta G \tag{10}$$

where $\Delta G = G_{-} - G_{+}$ is the residual gain difference between cross- and co-slant receive channels after ordinary calibration. For each $|\Delta G|$, both signs are evaluated and the larger RMSE is reported. Microphysical sensitivity is tested by varying physical canting spread and by training/testing across Brandes and Thurai axis-ratio relations. Cross-slant detectability is assessed with a first-order signal-to-noise relation. Let N_{+} and N_{-} denote the co- and cross-slant receiver-noise powers, then the cross-slant signal-to-noise ratio can be written as

$$\mathrm{SNR_{-,dB}} = \mathrm{SNR_{+,dB}} + \mathrm{SLDR_{hyd,dB}} + 10\log_{10}\left(\frac{N_{+}}{N_{-}}\right) \tag{11}$$

For comparable channel noise powers, $\mathrm{SNR_{-,dB}} \approx \mathrm{SNR_{+,dB}} + \mathrm{SLDR_{hyd,dB}}$. Thus, an SLDR of −25 dB requires a co-slant SNR well above 25 dB for the cross-slant return to be measurable. Finite polarization isolation imposes an additional lower bound on measurable SLDR. If I is the effective isolation in dB, the observed cross-to-co ratio can be approximated as

$$\mathrm{SLDR_{obs}} \approx 10\log_{10}\left(10^{\mathrm{SLDR_{hyd}}/10} + 10^{-I/10}\right) \tag{12}$$

This expression does not replace a full polarimetric calibration model, but it identifies the leakage floor below which the hydrometeor-generated SLDR cannot be separated from instrumental cross-channel leakage. Effective isolation levels of 25, 30, 35, and 40 dB therefore correspond to approximate leakage floors of -25, -30, -35, and -40 dB, respectively.

3 Results

3.1 Organization of the Z_{+}–SLDR observation space

In the slant basis, the orthogonal return is controlled by H/V backscattering contrast rather than by total echo power alone. The single-particle response in Fig. 2a shows that nearly spherical small drops generate little cross-slant power, whereas larger oblate drops produce stronger SLDR. Frequency modulates this relationship because the scattering regime changes as raindrop size becomes comparable to the radar wavelength. At Ka and especially W band, non-Rayleigh scattering introduces diameter-dependent structure in the single-particle SLDR curve. These features affect the detailed mapping between SLDR and drop diameter, but they do not change the basis-rotation mechanism.

After integration over DSDs, the same mechanism produces an organized Z_{+}-SLDR microphysical space. Although Ka-band non-Rayleigh structure appears in the single-particle response, it is smoothed by realistic drop spectra because the number concentration decreases rapidly at large diameters. If SLDR contained no information beyond reflectivity, samples with similar Z_{+} would collapse into an unstructured band. Instead, Fig. 2b shows that D_m varies systematically across the Z_{+}-SLDR plane: at fixed reflectivity, a larger SLDR corresponds to a larger characteristic drop size. Figure 2c shows the complementary variation of N_w, indicating that the two-dimensional space separates size-driven and concentration-driven changes in reflectivity. The rain-rate and total-concentration fields in Figs. 2d and 2e show the same organization from different microphysical perspectives.

The displayed Z_{+}–SLDR plane also contains physically empty regions. These regions correspond to combinations of reflectivity and SLDR that are not produced by the sampled liquid-rain gamma DSDs within the evaluation domain, rather than to missing samples. The lower-SLDR boundary should be interpreted as an approximate observability limit: below this range, the hydrometeor-generated cross-slant return is expected to become increasingly controlled by receiver noise and polarization leakage.

https://doi.org/10.5194/egusphere-2026-3198
Preprint. Discussion started: 21 August 2026

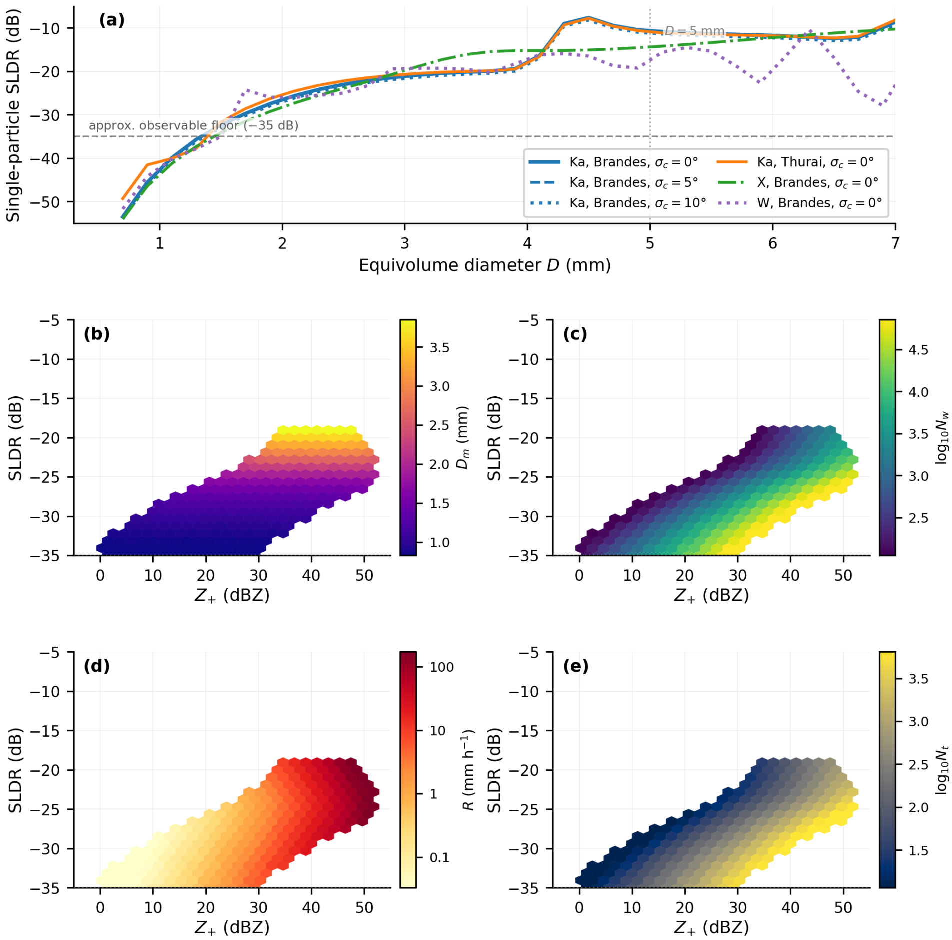

Figure 2. Scattering basis and information content of the Z_+–SLDR observation space. (a) Single-particle SLDR as a function of equivolume diameter for selected frequencies, raindrop shape relations, and physical canting-angle spreads about horizontal alignment. The radar basis is fixed at $+45°/-45°$ for all curves, and the dashed horizontal line marks an approximate −35 dB observability floor. The vertical line marks $D = 5$ mm, above which Ka-band single-particle resonance effects become more visible but which contributes little to typical DSD number concentration. (b–e) Ka-band gamma-DSD samples with $\mu = 3$, horizontally aligned baseline drops ($\sigma_c = 0°$), and $R \le 200$ mm h^{-1} projected into the Z_+–SLDR plane and displayed over SLDR ≥ -35 dB as hexagonal bins. Colors indicate median (b) mass-weighted mean diameter D_m, (c) normalized intercept parameter N_w, (d) rain rate R, and (e) total concentration N_t in each bin.

3.2 Retrieval information content in the controlled gamma ensemble

The organized Z_+–SLDR structure suggests that SLDR should reduce the DSD ambiguity left by reflectivity alone. Figure 3 tests this directly with the MLP diagnostic. The Z-only network collapses much of the unresolved D_m variability toward a conditional mean, producing broad scatter and D_m RMSE of 0.672 mm (Fig. 3a). The

https://doi.org/10.5194/egusphere-2026-3198
Preprint. Discussion started: 21 August 2026

same limitation is less visually dramatic for $\log_{10}R$ because rain rate is strongly correlated with reflectivity, but the Z-only retrieval still retains systematic spread and RMSE of 0.163 (Fig. 3d).

Adding SLDR largely removes this ambiguity in the noise-free information-content limit. The clean Z–SLDR retrievals reduce D_m RMSE from 0.672 to 0.012 mm and $\log_{10}R$ RMSE from 0.163 to 0.009 (Figs. 3b and 3e). This case is not intended as a field-performance estimate; it shows the upper bound of the measurement coordinate in the adopted scattering model.

With 1 dB SLDR uncertainty, the paired Z–SLDR vector still reduces D_m RMSE from 0.672 to 0.243 mm and $\log_{10}R$ RMSE from 0.163 to 0.055 (Figs. 3c and 3f). Back-transformed raw-R RMSE decreases from 12.0 to 5.8 mm h^{-1} within the same evaluation domain. The D_m retrieval degrades more strongly than $\log_{10}R$ because it relies more directly on the drop-shape information carried by SLDR, whereas rain rate remains partly constrained by reflectivity.

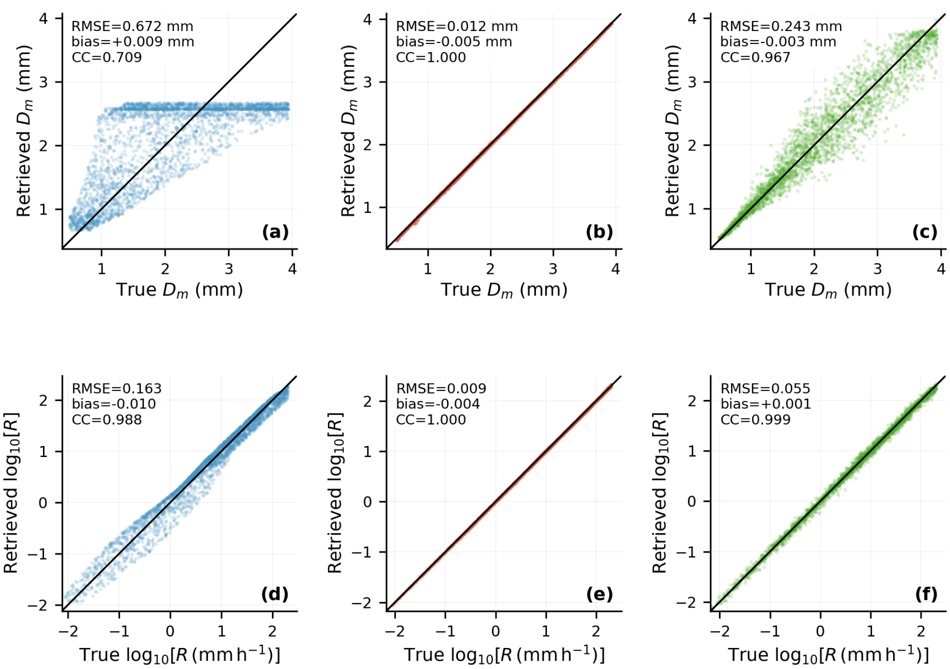

Figure 3. Comparison of retrieved and true values for an independent testing subset of the Ka-band gamma-DSD ensemble using the MLP diagnostic. The top row shows D_m retrieval and the bottom row shows $\log_{10}R$ retrieval. Columns show (a,d) Z-only retrieval, (b,e) noise-free Z–SLDR retrieval, and (c,f) Z–SLDR retrieval with 1 dB Gaussian random error added to SLDR at test time; the noisy-SLDR network is trained with matching SLDR-noise augmentation. Panel statistics report RMSE, mean bias (retrieved minus true), and Pearson correlation coefficient (CC).

3.3 Consistency across DSD priors and observed spectra

The same sign of improvement persists when the DSD prior is replaced by observed spectra or when the gamma-shape prior is relaxed. These experiments are consistency checks of the simulated measurement coordinate rather than independent radar validation, because both Z_+ and SLDR are still forward modeled from the DSDs using the same scattering framework. Figure 4 summarizes these checks in terms of the RMSE ratio, defined as

https://doi.org/10.5194/egusphere-2026-3198
Preprint. Discussion started: 21 August 2026

$\mathrm{RMSE}(Z_+ + \mathrm{SLDR}, 1\ \mathrm{dB})/\mathrm{RMSE}(Z_+\ \mathrm{only})$. Values below 1 therefore indicate that SLDR reduces retrieval error relative to reflectivity alone.

For the primary targets D_m and $\log_{10}R$ (Fig. 4a,b), every experiment remains below 1. The D_m ratio ranges from 0.34 to 0.62, and the $\log_{10}R$ ratio ranges from 0.29 to 0.60. The fixed-μ gamma benchmark gives ratios of 0.36 for D_m and 0.34 for $\log_{10}R$, while the variable-μ gamma test remains favorable with ratios of 0.38 and 0.40, respectively. This indicates that the added information is not tied to a single fixed-shape gamma prior. The observed Nanjing 2DVD subset, which is most directly connected to the target deployment environment, also remains favorable under 1 dB SLDR uncertainty, with ratios of 0.62 for D_m and 0.42 for $\log_{10}R$.

The public EPFL HyMeX and NASA IFLOODS Parsivel checks provide external DSD-sampling tests. For EPFL HyMeX SOP3 station 20, the RMSE ratio is 0.34 for D_m and 0.29 for $\log_{10}R$; for NASA IFLOODS apu01, the corresponding ratios are 0.43 and 0.60. The absolute error reductions differ among data sets because the sampled rain regimes and DSD variability differ, but the sign of the information gain is consistent. As a raw-rain-rate check, the Nanjing 2DVD subset also shows the same behavior, with raw-R RMSE decreasing from 1.95 to 1.49 under 1 dB SLDR error.

Additional retrieval targets show a similar pattern. Figure 4c shows the RMSE-ratio metric for $\log_{10}N_w$, $\log_{10}\mathrm{LWC}$, and $\log_{10}N_t$. The improvement remains systematic for $\log_{10}N_w$ and $\log_{10}\mathrm{LWC}$ across all four available data sets, with ratios of 0.30–0.58 and 0.31–0.66, respectively. The gain for $\log_{10}N_t$ is more variable, ranging from 0.30 for the fixed-μ gamma case to 0.88 for NASA IFLOODS. This weaker improvement is physically plausible because number-concentration proxies are more sensitive to DSD-prior mismatch and sampling differences than D_m or rain rate.

The ratios in Fig. 4 should therefore be interpreted as information-content diagnostics under a common scattering model, not as site-independent operational retrieval errors. Their role is to test whether the Z_+–SLDR coordinate remains informative when the DSD sampling prior changes. The absolute performance of a field radar will also depend on attenuation, cross-slant signal-to-noise ratio, polarization isolation, relative channel calibration, scan geometry, and hydrometeor screening. Within this controlled forward-modeling framework, Fig. 4 shows that the simulated SLDR information gain is not limited to the baseline fixed-μ gamma ensemble.

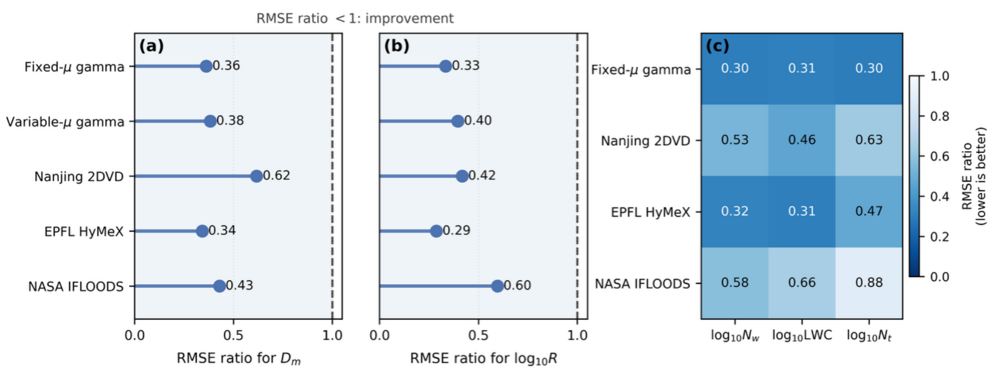

Figure 4. Consistency summary across DSD priors, local observed spectra, and public observed-DSD data sets. Panels (a) and (b) show RMSE ratios for D_m and $\log_{10}R$, respectively, defined as the RMSE from the Z_++SLDR retrieval with 1 dB SLDR uncertainty divided by the corresponding Z_+-only RMSE. Values below 1 indicate that SLDR reduces the retrieval error relative to reflectivity alone. The checks include the fixed-μ gamma benchmark, a variable-μ

https://doi.org/10.5194/egusphere-2026-3198
Preprint. Discussion started: 21 August 2026

gamma prior, local Nanjing 2DVD spectra, and public EPFL HyMeX and NASA IFLOODS Parsivel spectra. Panel (c) shows the same RMSE-ratio metric for additional logarithmic retrieval targets. These observed-DSD tests are consistency checks of the forward-modeled measurement coordinate rather than independent radar validation.

3.4 Observability constraints for field implementation

The preceding retrieval diagnostics establish the potential information content of the Z_+–SLDR coordinate under the forward-modeling framework. For a field radar, this information is useful only if the hydrometeor-generated orthogonal-slant return can first be distinguished from receiver noise and polarization leakage. The first-order relations in Sect. 2.4 provide this detectability constraint by linking the cross-slant SNR to the co-slant SNR, hydrometeor SLDR, channel-noise levels, and effective polarization isolation. They are used here as practical interpretation criteria, rather than as a separate radar-system simulation.

Given this detectability requirement, Fig. 5 focuses on how the Z_+–SLDR retrieval degrades once an SLDR estimate is available. The perturbations include random SLDR uncertainty, relative co-/cross-slant gain bias, canting-angle spread, and uncertainty in the raindrop axis-ratio relation. The results should therefore be interpreted as conditional sensitivity tests of the Z_+–SLDR information content, rather than as a full prediction of field-radar performance.

Random SLDR uncertainty and systematic gain bias affect the retrieval differently. Random uncertainty represents scatter in a noise-corrected SLDR estimate. When this uncertainty is represented during training through matching noise augmentation, the Z_+–SLDR retrieval degrades gradually but remains informative: Fig. 5a shows D_m RMSE of about 0.24 mm at 1 dB SLDR noise and about 0.53 mm at 3 dB, both below the Z_+-only baseline of 0.672 mm. The same behavior appears for $\log_{10}R$ in Fig. 5e, with weaker degradation because rain rate remains partly constrained by reflectivity.

Systematic relative co-/cross-slant gain bias is more restrictive because it shifts samples coherently in the Z_+–SLDR plane. As shown in Figs. 5b and 5f, the Z_+–SLDR retrieval remains beneficial for small gain biases, but the error grows rapidly as the residual bias increases and can approach or exceed the Z_+-only baseline. This result identifies relative co-/cross-slant calibration as a central requirement for field use. A stable SLDR zero point is needed because a systematic channel-gain error can be misinterpreted as microphysical variability.

Figures 5c, 5d, 5g, and 5h examine microphysical-model sensitivity. Canting-angle spreads of 5°–10° have little effect in this controlled gamma experiment, indicating that moderate zero-mean physical canting does not dominate the simulated SLDR information content. The axis-ratio test shows a larger but physically interpretable sensitivity: same-model Brandes-to-Brandes and Thurai-to-Thurai retrievals remain nearly error-free, whereas cross-model cases introduce larger errors because SLDR is controlled by the H/V backscattering contrast. This behavior supports the interpretation that SLDR carries information of raindrop shape, while also identifying the effective drop shape–size relation as a systematic uncertainty for field interpretation.

https://doi.org/10.5194/egusphere-2026-3198
Preprint. Discussion started: 21 August 2026

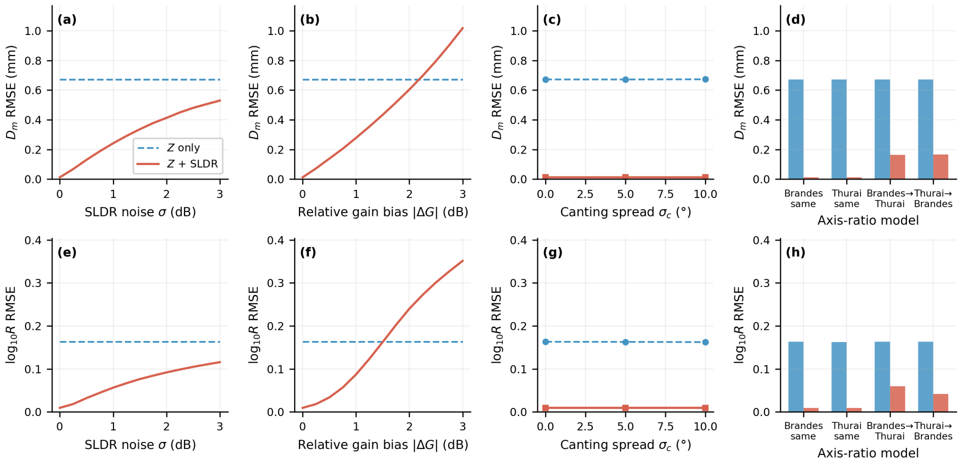

Figure 5. Observability envelope for the Ka-band Z_+–SLDR neural-network information-content retrieval. Panels show retrieval RMSE for Z-only and Z–SLDR retrievals under random SLDR uncertainty, systematic relative co-/cross-slant gain bias, canting-angle spread, and raindrop axis-ratio model consistency. The top row shows D_m RMSE for (a) SLDR noise, (b) gain bias, (c) canting-angle spread, and (d) axis-ratio model consistency. The bottom row shows the corresponding $\log_{10}R$ RMSE for (e)–(h). Here $|\Delta G|$ denotes the magnitude of the relative co-/cross-slant gain bias; for each magnitude, the plotted value is the larger RMSE from the positive and negative bias cases. In panels (d) and (h), same-model cases train and test with the same axis-ratio relation, whereas cross-model cases train with one relation and test with the other.

3.5 Frequency transferability

The 45° basis-rotation mechanism is not specific to Ka band. Changing the radar frequency does not change the geometric projection that produces the orthogonal-slant return, but it does change the magnitude and diameter dependence of the single-particle scattering response, as well as the practical detectability of the weak cross-slant signal. At conventional S-, C-, and X-band weather-radar wavelengths, full H/V dual-polarization measurements are already well established for research and operational precipitation monitoring. SLDR is therefore not proposed as a replacement for conventional dual-polarization operation. Its main relevance is for radar architectures, particularly compact millimeter-wave and cloud-radar systems, in which a slant transmit state and an orthogonal receive channel may be easier to implement than full H/V polarimetry.

At W band, non-Rayleigh effects begin at smaller drop diameters, so the single-particle SLDR response can be more structured than at Ka band (Figure 2a). Figure 6 shows, however, that the DSD-integrated Z_+–SLDR mapping remains ordered with D_m for the same gamma ensemble. This occurs because realistic DSD integration weights the response toward the more numerous smaller and moderate-size drops, smoothing part of the single-particle oscillatory structure. For this ensemble, the Spearman rank correlation between SLDR and D_m is 1.000 for both Ka and W bands. This result should be interpreted as a consistency check of the basis-rotation mechanism after DSD integration, not as evidence that W-band rainfall SLDR would have the same observability or retrieval performance as the Ka-band case. A practical W-band implementation would require a separate assessment of attenuation, receiver sensitivity, polarization isolation, and calibration stability.

https://doi.org/10.5194/egusphere-2026-3198
Preprint. Discussion started: 21 August 2026

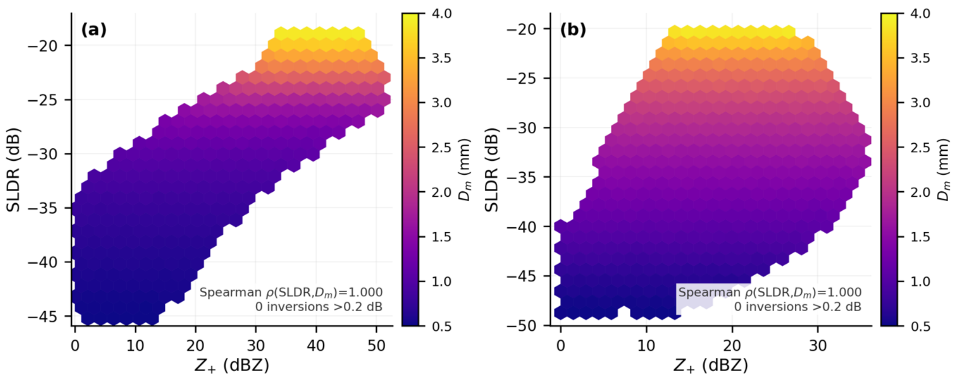

Figure 6. Frequency transferability of the DSD-integrated SLDR information space. The Z_+–SLDR mapping at (a) Ka band (35 GHz) and (b) W band (94 GHz) for the same gamma-DSD ensemble are compared, with colors indicating median D_m.

4 Discussion

The results identify SLDR as a physically distinct radar coordinate for liquid-rain microphysics. In a fixed slant-linear basis, the H/V scattering anisotropy of oblate raindrops is projected into the orthogonal-slant receive channel. SLDR is therefore not a transformation of reflectivity, but a polarization power ratio whose sensitivity arises from the shape-dependent contrast between horizontal and vertical co-polar backscattering amplitudes. The Ka-band simulations show that the joint Z_+–SLDR space organizes DSD variability by characteristic drop size and concentration, and the retrieval diagnostics show that this additional coordinate reduces the ambiguity that remains when rainfall is sensed by reflectivity alone.

This interpretation is consistent with the broader view that liquid-rain DSD variability cannot generally be constrained by a single radar moment. Reflectivity is strongly weighted toward larger drops, but a given reflectivity can result from different combinations of drop size and number concentration. SLDR provides a complementary coordinate that is linked to raindrop shape and characteristic size. In this sense, the proposed measurement brings suitable single-transmit, dual-receive radars closer to a two-coordinate description of rain microphysics, consistent with moment-normalization studies showing that much of the structured variability in normalized DSDs can be represented using more than one reference moment (Morrison et al., 2019). This does not imply that SLDR fully determines the DSD, but it explains why the added information is physically meaningful rather than merely statistical.

The practical appeal of the approach is that it may be implemented on radar architectures that already transmit a single polarization and receive co- and cross-polarized components. A slant basis can be realized by feed or antenna rotation, or by polarization synthesis where supported, rather than by replacing the system with a conventional H/V dual-polarization weather radar. SLDR-mode operation has already been demonstrated with a 35 GHz scanning cloud radar by rotating a conventional LDR configuration into the slant-linear basis (Teisseire et al., 2024). The rainfall application considered here would require controlled slant-polarization operation and calibrated co-/cross-slant receive channels, but not full H/V dual-polarization transmission.

The main limitation is that the liquid-rain SLDR signal is weak. The hydrometeor-generated cross-slant return must exceed receiver-noise and polarization-leakage floors, and the relative co-/cross-slant gain must be stable

https://doi.org/10.5194/egusphere-2026-3198
Preprint. Discussion started: 21 August 2026

enough for SLDR to remain a microphysical observable rather than an instrumental artifact. The sensitivity experiments show that random SLDR uncertainty degrades the retrieval gradually, whereas systematic gain bias is more restrictive because it shifts samples coherently in the Z_+–SLDR plane. The axis-ratio tests also show that SLDR is sensitive to the assumed drop shape–size relation, as expected from its dependence on H/V backscattering contrast. Field interpretation will therefore require attention not only to instrumental calibration, but also to the effective raindrop-shape model.

The present study is a forward-modeled information-content analysis rather than a direct radar validation. The observed-DSD experiments test whether the simulated Z_+–SLDR coordinate remains informative across different DSD priors and sampling regimes, but both radar variables are still calculated from measured spectra using the same scattering framework. A direct field test should compare collocated slant-polarized radar observations with independent DSD measurements under documented polarization isolation, relative channel calibration, cross-slant signal-to-noise ratio, attenuation screening, scan geometry, and liquid-phase quality control. Such a test would determine whether the simulated information gain can be realized by an actual radar system and would help separate errors due to instrumentation, scattering assumptions, attenuation, beam filling, and sampling mismatch.

5 Conclusions

This study evaluated whether a fixed slant-linear polarization basis can provide useful liquid-rain microphysical information for single-transmit, dual-receive millimeter-wave radars. Using explicit T-matrix scattering calculations and controlled retrieval diagnostics, we showed that a +45°/−45° slant basis projects the H/V co-polar backscattering contrast of oblate raindrops into an orthogonal-slant return. The resulting SLDR is a distinct polarization observable, rather than a transformation of reflectivity, with sensitivity tied to the raindrop-shape-dependent difference between horizontal and vertical co-polar backscattering amplitudes.

In the Ka-band gamma-DSD ensemble, the joint Z_+–SLDR plane organizes DSD variability by characteristic drop size and concentration. Adding SLDR with 1 dB uncertainty reduces the independent-test D_m RMSE from 0.672 to 0.243 mm, and reduces the $\log_{10} R$ RMSE from 0.163 to 0.055 relative to Z_+ alone. Consistency checks using Nanjing 2DVD spectra, EPFL HyMeX Parsivel spectra, NASA IFLOODS Parsivel spectra, a variable-shape gamma prior, and additional microphysical targets show the same sign of improvement, indicating that the simulated information gain is not limited to the baseline gamma prior.

The practical use of rainfall SLDR is constrained by cross-slant detectability, polarization isolation, relative co-/cross-slant gain stability, and raindrop-shape assumptions. Random SLDR uncertainty degrades the retrieval gradually, whereas systematic gain bias and leakage floors can more strongly limit the interpretation of SLDR as a microphysical coordinate. The W-band consistency check shows that the basis-rotation mechanism is not specific to Ka band, although practical performance at different frequencies must be evaluated with instrument-specific noise, attenuation, and calibration characteristics. Overall, the results support SLDR as a testable measurement coordinate for suitable single-transmit, dual-receive millimeter-wave radars, provided that the hydrometeor-generated cross-slant return is measurable and well calibrated.

Code and data availability

The processed NJU/Nanjing 2DVD integrated scattering products generated for this study have been archived at Zenodo (https://zenodo.org/records/20070082). The public EPFL HyMeX station 20 Parsivel data are available

https://doi.org/10.5194/egusphere-2026-3198
Preprint. Discussion started: 21 August 2026

from Zenodo (Berne et al., 2023), and the NASA IFLOODS apu01 Parsivel data are available from the NASA PMM/GPM Ground Validation public archive (NASA, 2025).

Author contributions

HH designed the study, developed the scattering and retrieval experiments, prepared the figures, and wrote the manuscript draft. CL and WZ contributed to data processing and interpretation. KZ contributed to the radar-meteorological interpretation. XW contributed to the neural-retrieval methodology. All authors reviewed and edited the manuscript.

Competing interests

The authors declare that they have no conflict of interest.

Acknowledgments

We acknowledge the EPFL HyMeX team and the NASA PMM/GPM Ground Validation program for making public disdrometer data available for independent consistency checks. AI-assisted tools were used for code assistance, document restructuring, and language editing; all scientific interpretation, calculations, and final text were checked by the authors.

Financial support

This work is supported by the National Natural Science Foundation of China (Grant 42422501), the AI & AI for Science Project of Nanjing University (Grant 020714380231), and the Jianghuai Meteorological Joint Project of Anhui Natural Science Foundation (Grant 2408055UQ002).

References

Berne, A., Grazioli, J., Raupach, T., & Schleiss, M. (2023). *EPFL HYMEX_LTE_SOP3 20 disdrometer station data [Dataset]* (https://doi.org/https://doi.org/10.5281/zenodo.10360981

Brandes, E. A., Zhang, G., & Vivekanandan, J. (2002). Experiments in Rainfall Estimation with a Polarimetric Radar in a Subtropical Environment. *Journal of Applied Meteorology*, *41*(6), 674–685. https://doi.org/10.1175/1520-0450(2002)041<0674:EIREWA>2.0.CO;2

Bringi, V. N., & Chandrasekar, V. (2001). *Polarimetric Doppler weather radar: principles and applications*. Cambridge University Press.

Bringi, V. N., Chandrasekar, V., Hubbert, J., Gorgucci, E., Randeu, W. L., & Schoenhuber, M. (2003). Raindrop Size Distribution in Different Climatic Regimes from Disdrometer and Dual-Polarized Radar Analysis. *Journal of the Atmospheric Sciences*, *60*(2), 354–365. https://doi.org/10.1175/1520-0469(2003)060<0354:RSDIDC>2.0.CO;2

Görsdorf, U., Lehmann, V., Bauer-Pfundstein, M., Peters, G., Vavriv, D., Vinogradov, V., & Volkov, V. (2015). A 35-GHz Polarimetric Doppler Radar for Long-Term Observations of Cloud Parameters—Description of System and Data Processing. *Journal of Atmospheric and Oceanic Technology*, *32*(4), 675–690. https://doi.org/https://doi.org/10.1175/JTECH-D-14-00066.1

Kollias, P., Clothiaux, E. E., Miller, M. A., Albrecht, B. A., Stephens, G. L., & Ackerman, T. P. (2007). Millimeter-Wavelength Radars: New Frontier in Atmospheric Cloud and Precipitation Research. *Bulletin of the American Meteorological Society*, *88*(10), 1608–1624. https://doi.org/https://doi.org/10.1175/BAMS-88-10-1608

https://doi.org/10.5194/egusphere-2026-3198
Preprint. Discussion started: 21 August 2026

Leinonen, J. (2014). High-level interface to T-matrix scattering calculations: architecture, capabilities and limitations. *Optics Express*, *22*(2), 1655–1660. https://doi.org/10.1364/OE.22.001655

Liebe, H. J., Hufford, G. A., & Manabe, T. (1991). A model for the complex permittivity of water at frequencies below 1 THz. *International Journal of Infrared and Millimeter Waves*, *12*(7), 659–675. https://doi.org/10.1007/bf01008897

Matrosov, S. Y. (2021). Polarimetric Radar Variables in Snowfall at Ka- and W-Band Frequency Bands: A Comparative Analysis. *Journal of Atmospheric and Oceanic Technology*, *38*(1), 91–101. https://doi.org/https://doi.org/10.1175/JTECH-D-20-0138.1

Matrosov, S. Y., Mace, G. G., Marchand, R., Shupe, M. D., Hallar, A. G., & McCubbin, I. B. (2012). Observations of Ice Crystal Habits with a Scanning Polarimetric W-Band Radar at Slant Linear Depolarization Ratio Mode. *Journal of Atmospheric and Oceanic Technology*, *29*(8), 989–1008. https://doi.org/https://doi.org/10.1175/JTECH-D-11-00131.1

Morrison, H., Kumjian, M. R., Martinkus, C. P., Prat, O. P., & van Lier-Walqui, M. (2019). A General N-Moment Normalization Method for Deriving Raindrop Size Distribution Scaling Relationships. *Journal of Applied Meteorology and Climatology*, *58*(2), 247–267. https://doi.org/10.1175/jamc-d-18-0060.1

NASA. (2025). *NASA IFLOODS apu01 Parsivel disdrometer data in the DISDRODB raw archive [Dataset]* (https://doi.org/https://pmm-gv.gsfc.nasa.gov/pub/DISDRODB/RAW/NASA/IFLOODS/data/apu01/

Sandford, C., Illingworth, A., & Thompson, R. (2017). The potential use of the linear depolarisation ratio to distinguish between convective and stratiform rainfall to improve radar rain rate estimates. *Journal of Applied Meteorology and Climatology*, *56*(11), 2927–2940. https://doi.org/10.1175/JAMC-D-17-0014.1

Seliga, T. A., & Bringi, V. N. (1976). Potential Use of Radar Differential Reflectivity Measurements at Orthogonal Polarizations for Measuring Precipitation. *Journal of Applied Meteorology*, *15*(1), 69–76. https://doi.org/10.1175/1520-0450(1976)015<0069:PUORDR>2.0.CO;2

Teisseire, A., Seifert, P., Myagkov, A., Bühl, J., & Radenz, M. (2024). Determination of the vertical distribution of in-cloud particle shape using SLDR-mode 35 GHz scanning cloud radar. *Atmos. Meas. Tech.*, *17*(3), 999–1016. https://doi.org/10.5194/amt-17-999-2024

Thurai, M., & Bringi, V. N. (2005). Drop Axis Ratios from a 2D Video Disdrometer. *Journal of Atmospheric and Oceanic Technology*, *22*(7), 966–978. https://doi.org/10.1175/jtech1767.1

Ulbrich, C. W. (1983). Natural Variations in the Analytical Form of the Raindrop Size Distribution. *Journal of Climate and Applied Meteorology*, *22*(10), 1764–1775. https://doi.org/10.1175/1520-0450(1983)022<1764:Nvitaf>2.0.Co;2

Wen, L., Zhao, K., Wang, M., & Zhang, G. (2019). Seasonal Variations of Observed Raindrop Size Distribution in East China. *Advances in Atmospheric Sciences*, *36*(4), 346–362. https://doi.org/10.1007/s00376-018-8107-5

Zhang, G. (2016). *Weather Radar Polarimetry* (2nd ed.). CRC Press. https://doi.org/10.1201/9781315374666-7